Strojniški vestnik - Journal of Mechanical Engineering 68(2022)9, 560-570
DOI:10.5545/sv-jme.2022.69
Original Scientific Paper
Received for review: 2022-02-21
Received revised form: 2022-07-01
Accepted for publication: 2022-07-11

Limit-protection Method for the Workspace of a Parallel Power Head

Yanbing Ni[1,*] – Wenliang Lu[2] – Shilei Jia[2] – Chenghao Lu[2] – Ling Zhang[2] – Yang Wen[1]
[1] Tianjin University, School of Mechanical Engineering, China
[2] Key Laboratory of Mechanism Theory and Equipment Design of Ministry of Education, China

The end pose of a one-translation two-rotation (1T2R) parallel mechanism is a mapping of the servo motor action in the joint space. Because it is difficult to obtain information about the end attitude state, we have designed and implemented a simplified algorithm for determining the attitude of such a mechanism. The kinematic inverse solution of the robot and the modelling analysis of the workspace are carried out. From this, it is deduced that the length transformation of the three branch chains of the mechanism reflects the position and attitude of the end-motion platform. Based on this algorithm, the limit protection of a parallel power head under arbitrary configuration is realized. The correctness of the calculation method is verified by simulation. Finally, based on the software and hardware conditions of an existing control system, experimental verification is carried out. The experimental results show that the simplified algorithm can implement limit protection for this type of machine.

Keywords: parallel power head, modelling, workspace analysis, position and pose judgment, limit-protection

Highlights
- *The kinematics of the 1T2R head are analysed, and the workspace of the mechanism is obtained.*
- *A new simplified algorithm for position and attitude judgment is proposed.*
- *The new simplified algorithm of position and attitude judgment is combined with the mechanism control system to realize a fast limit.*
- *The algorithm is verified with simulation and experimental data.*

0 INTRODUCTION

Due to its compact structure, high stiffness to mass ratio, high precision, and good dynamic characteristics [1] and [2], the parallel power head has been of interest to both academia and the manufacturing industry and has been widely used in high-end manufacturing fields, such as large aircraft structural parts [3].

The working space is the key index for evaluating the performance of parallel power heads. Unlike tandem robots, which are driven by a series of connecting rods and rotating joints in series, parallel power heads are connected by at least two independent kinematic chains. Although the working space is relatively small, their structure is precise and compact with high repetitive positioning accuracy [4] and [5]. Workspaces can be partitioned in a number of ways, depending on performance requirements and selected parameters [6]. The factors influencing the size and shape of the workspace include the constraints of the length of the branch chain, the rotation angle, and the size of the revolute joint [7] and [8]. The methods used for the analysis of the workspace include the geometric, numerical [5], and discretization methods [9] and [10]. Gui et al. [11] proposed a reliability mathematical model based on random probability and presented a measurement and calculation method for the evaluation of the reliability level of mechanism motion. Shao et al. [12] analysed the new spatial-planer parallel mechanism using geometric methods and verified that it has good accuracy and efficiency. Kaloorazi et al. [13] used the structural geometry method to determine the maximum non-singularity workspace of a 3-degree of freedom (3-DOF) parallel mechanism, and Huang et al. [9] obtained the workspace of the Stewart-Gough manipulator by a discrete method. The scientific community has also made many achievements in numerical method research. Zhang [14] et al. used the fast search method to calculate the workspace volume and took it as the optimization objective function. In addition, Gao and Zhang [15] and Zhu et al. [16] used the modified boundary search method to obtain the workspace of a parallel mechanism. Farzaneh-Kaloorazi et al. [17] used an interval analysis approach for the barrier-free working space of a parallel mechanism. Majid [18] et al. analysed the workspace of a three-prismatic-prismatic-spheric-revolute (3-PPSR) manipulator using the numerical method and found that three regions in the workspace corresponded to the postures of a type of manipulator.

In order to make more reasonable and effective use of the existing working space and ensure the safe and reliable operation of the parallel power

*Corr. Author's Address: Tianjin University, School of Mechanical Engineering, China, niyb5812@tju.edu.cn

head, the method of trajectory planning and space limitation is often adopted [19] and [20]. Khoukhi et al. [21] proposed a multi-objective dynamic trajectory planning method for the parallel mechanism under the constraints of task, workspace, and mechanism with the help of the discrete augmented Lagrangian technique. Reveles et al. [22] proposed a kinematic redundant parallel robot joint trajectory planning method using a feasibility map, which plans the joint trajectory while avoiding parallel singularities through the graphical evaluation of the robot pose related to four working modes. Dash et al. [23] proposed a numerical path planning method to avoid the singularity of the mechanism in the accessible workspace of a parallel robot by clustering the singularities and using the local routing method based on Grassmann line geometry to avoid the singularities. Iqbal et al. [24] discussed two complex control strategies: computational torque control (CTC) and variable structure control (VSC) and improved the trajectory-tracking performance of the robot. Manzoor et al. [25] integrated the functions of mechanical computer-aided design (CAD) and robot CAD into the same platform and achieved the accurate control of the robot through various three-dimensional models in the platform. Alam et al. [26] considered two different methods based on sliding mode control (SMC) to achieve the nonlinear control of an elastic joint robot. This control method enables the robot to obtain a locally stable closed-loop system.

Because the pose of the end of the one-translation two-rotation (1T2R) parallel mechanism in the operation space is a nonlinear mapping of the motion of the servo motor in the joint space, the modelling and calculation process is complicated, the motion controller takes a long time. It is therefore impossible to realize the real-time operation to prevent exceeding the limit during the operation of the mechanism. The purpose of this paper is to propose a simplified algorithm for position and attitude judgment, which can greatly reduce the calculation amount of limit, and realize the limit protection of the 1T2R parallel power head through a combination of software and hardware. Firstly, the inverse kinematics analysis was carried out, and the mapping relationship between the terminal pose of the mechanism and each input value was constructed based on the inverse kinematics model. Then, according to the mechanism structure, scale parameters, range of motion of each pair, interference and other constraints, the working space of 1T2R power head was determined. By analysing and summarizing the motion rules of 1T2R power head, a simplified algorithm for judging the position and pose of 1T2R power head was obtained, which was used to realize the limit protection of the 1T2R head. Finally, the algorithm was verified via experimentation.

1 KINEMATIC ANALYSIS

The position inverse solution of the 1T2R head is to solve the rod length quantity of each branch chain motion joint by knowing the positional parameters of the end reference point of the tool providing the theoretical model for mechanism error analysis and control.

1.1 Machine Tool Profile

As shown in Fig. 1, a 1T2R mechanism is a parallel mechanism with one translational and two rotational degrees of freedom. A 1T2R power head is composed of a moving platform, a static platform, and three RPS branch chains, in which R, P, and S represent revolute joints, active prismatic pairs and spherical joints, respectively. One end of each RPS branch chain is connected to the moving platform through a spherical joint, and the other end is connected to the static platform through a revolute joint. The motorized spindle is installed on the moving platform and the active prismatic pair is driven by a servo motor.

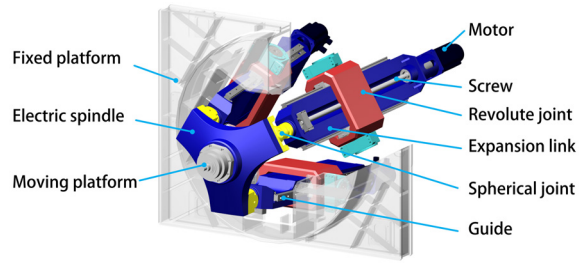

Fig. 1. *Model of 1T2R spindle head*

1.2 Inverse Kinematic Solution

The power head of the 1T2R mechanism diagram is shown in Fig. 2, A_i and B_i represent the centres of the spherical joint and the revolute joint, respectively; $\Delta A_1A_2A_3$ and $\Delta B_1B_2B_3$ are equilateral triangles; points O' and O are the geometric centres of the two triangles; the moving platform is represented by $\Delta A_1A_2A_3$; the static platform is represented by the plane of $\Delta B_1B_2B_3$; point P is the tip at the end of the mechanism; e is the distance from P to the plane of the moving platform; a, b are the circumcircle radii of the moving and static platform, respectively; l represents the initial branch length.

The fixed and moving coordinate systems $O-xyz$ and $O'-x'y'z'$ are established at the centre O and O' of the fixed and moving platforms, respectively. In the initial position, the z' axis and z axis are perpendicular to the planes $A_1A_2A_3$ and$B_1B_2B_3$, respectively, as shown in Fig. 2. The x' axis and x axis are along the $\overrightarrow{A_3A_2}$ direction and $\overrightarrow{B_3B_2}$, respectively. The y' axis and y axis are determined according to the right-hand rule. α and β represent rotation about the x axis and y axis, respectively.'

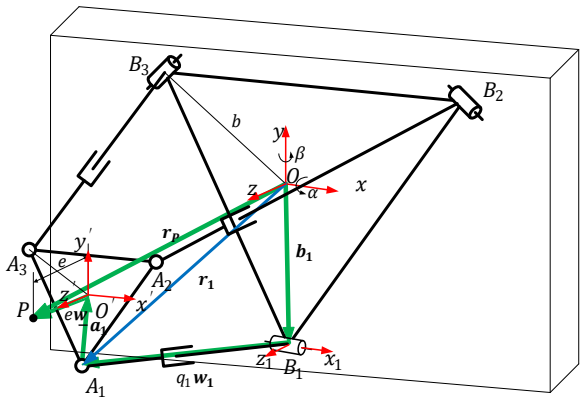

Fig. 2. *Mechanism sketch of 1T2R mechanism*

The attitude transformation matrix of $O'-x'y'z'$ in the connected body coordinate system of a moving platform relative to $O-xyz$ in the static platform coordinate system is R:

$$\begin{aligned}\mathbf{R} &= \mathrm{Rot}(z,\psi)\,\mathrm{Rot}(x,\theta)\,\mathrm{Rot}(z,\phi)\\ &= \begin{bmatrix} c\psi c\phi - s\psi c\theta s\phi & -c\psi s\phi - s\psi c\theta c\phi & s\psi s\theta \\ s\psi c\phi + c\psi c\theta s\phi & -s\psi s\phi + c\psi c\theta c\phi & -c\psi s\theta \\ s\theta s\phi & s\theta c\phi & c\theta \end{bmatrix}\\ &= \begin{bmatrix}\mathbf{u} & \mathbf{v} & \mathbf{w}\end{bmatrix},\end{aligned} \tag{1}$$

where $s=\sin$, $c=\cos$, $\mathbf{u}$, $\mathbf{v}$, $\mathbf{w}$ represent the measurement of three coordinate axes of $O'-x'y'z'$ in the static platform coordinate system $O-xyz$, respectively, and $\mathbf{w}$ can be used to represent the tool attitude vector.

ψ, θ, ϕ are the precession angle, nutation angle and spin angle, respectively, which are related to α and β:

$$\begin{cases}\theta = \arccos(\cos\alpha\cos\beta)\\ \psi = \mathrm{atan2}\left(\dfrac{\cos\alpha\sin\beta}{\sin\theta}, \dfrac{\sin\alpha}{\sin\theta}\right)\end{cases}. \tag{2}$$

As shown in Fig. 2, the position vector of the tool point P at the end of the mechanism in the static platform coordinate system $O-xyz$ is:

$$\mathbf{r}_P = \begin{bmatrix}x_P & y_P & z_P\end{bmatrix}^{\mathrm{T}}. \tag{3}$$

The following vector equation can be obtained:

$$\mathbf{r}_P = \mathbf{b}_i + q_i\mathbf{w}_i - \mathbf{a}_i + e\mathbf{w} \quad i=1,2,3, \tag{4}$$

where $\mathbf{a}_i$, $\mathbf{b}_i$ is the position vector of A_i, B_i; $\mathbf{a}_i=\mathbf{R}\mathbf{a}_{i0}$; $\mathbf{b}_i = b\begin{bmatrix}\cos\varphi_i & \sin\varphi_i & 0\end{bmatrix}^{\mathrm{T}}$; $\mathbf{a}_{i0}$ is the measurement of A_i in the connected coordinate system of moving platform, $\mathbf{a}_{i0} = a\begin{bmatrix}\cos\varphi_i & \sin\varphi_i & 0\end{bmatrix}^{\mathrm{T}}$; φ_i is the structural angle of $\overrightarrow{O'A_i}$ and $\overrightarrow{OB_i}$ relative to x' axis and x axis respectively, $\varphi_i = 2\pi(i-1)/3-\pi/2$; q_i and $\mathbf{w}_i$ are the length of the branch chain and the unit vector, respectively.

Since the revolute joint will restrict the branch chain from moving along the x_i axis, dot product x axis direction unit vector $\boldsymbol{u}_{ix}=\begin{bmatrix}cos\varphi_i & sin\varphi_i & 0\end{bmatrix}^{\mathrm{T}}$ at both ends of Eq. (4):

$$\left(\mathbf{r}_P + \mathbf{a}_i - e\mathbf{w}\right)^{\mathrm{T}}\cdot\mathbf{u}_{ix} = 0. \tag{5}$$

Solve Eq. (5) to obtain

$$\begin{aligned} x_P &= \frac{a}{2}\sin(2\psi)(1-\cos\theta) + e\sin\psi\sin\theta,\\ y_P &= \frac{a}{2}\cos(2\psi)(1-\cos\theta) - e\cos\psi\sin\theta,\\ \phi &= -\psi. \end{aligned} \tag{6}$$

From Eq. (6)

$$\begin{cases} q_i = \left\|\mathbf{r}_P - \mathbf{b}_i + \mathbf{a}_i - e\mathbf{w}\right\| = \left\|\mathbf{r}_P - \mathbf{b}_i - \mathbf{s}_i\right\|\\ \mathbf{w}_i = \left(\mathbf{r}_P - \mathbf{b}_i - \mathbf{s}_i\right)/q_i \quad i=1,2,3 \end{cases}, \tag{7}$$

where $\mathbf{s}_i$ is the vector of the geometric centre of the spherical pairs pointing to the tool reference point in the static coordinate system, and $\mathbf{s}$ is the vector of the geometric centre of the spherical pairs pointing to the tool reference point in the moving coordinate system.

$$\mathbf{s}_i = \mathbf{R}\mathbf{R}_i\mathbf{s}, \mathbf{s} = \begin{bmatrix}0 & a & e\end{bmatrix}^{\mathrm{T}}, \tag{8}$$

$$\mathbf{R}_i = \begin{bmatrix} \cos(\varphi_i+\pi/2) & -\sin(\varphi_i+\pi/2) & 0\\ \sin(\varphi_i+\pi/2) & \cos(\varphi_i+\pi/2) & 0\\ 0 & 0 & 1\end{bmatrix}, \quad i=1,2,3. \tag{9}$$

2 WORKSPACE ANALYSIS

The constraints of the 1T2R head include its structure, scale parameters (a, b, l, e), motion range of each prismatic pair and interference. Workspace analysis

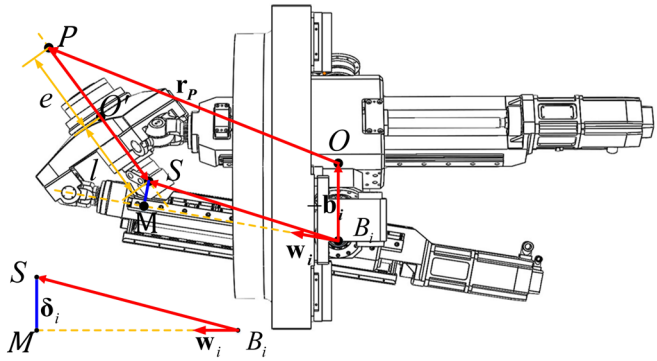

Fig. 3. *Interference position of 1T2R spindle head*

is used to determine the set of all reachable space position points of the tool reference point under the above constraints.

2.1 Constraint Analysis

The 1T2R power head is restricted by its own mechanical structure and other conditions and can only work within a certain space range. After analysing the structure of the 1T2R head, the constraint conditions are as listed in Table 1.

Table 1. *Restrictions of 1T2R mechanism*

Constraint type	Constraint value
Active prismatic pair length constraint	0.4 m ≤ q_i ≤0.915 m
Rotation angle constraint of revolute joint	–12° ≤ θ_i ≤ 3°
Angle constraint of spherical joint	$\lvert\alpha_i\rvert$ ≤ 45°, $\lvert\beta_i\rvert$ ≤ 90°
Interference between principal axis and branched chain	$\delta_i \geq 0.15$ m
Interference between tool point and table	$z_P \leq 1.250$ m

$q_{i\min}$ and $q_{i\max}$ are the maximum and minimum lengths of the active prismatic pairs, respectively; $\theta_{i\min}$ and $\theta_{i\max}$ are the maximum and minimum values of each revolute joint angle, respectively; $\alpha_{i\min}$ and $\beta_{i\max}$ are the maximum values of angles α and β of each spherical joint, respectively; δ_i is the linear distance from point S of the spindle end to the branch chain; $\delta_{i\min}$ is the minimum allowable actual linear distance between the spindle end and the branch chain. As shown in Fig. 3, δ_i can be obtained as follows:

$$\delta_i = \left|\mathbf{w}_i \times \mathbf{r}_{B_iS}\right| = \left|\mathbf{w}_i \times \left(\mathbf{r}_P - e\mathbf{w} - l\mathbf{w} - \mathbf{b}_i\right)\right|. \quad (10)$$

2.2 Workspace Description

A hierarchical processing approach can be used to divide the workspace into multiple subspaces. The boundary region of the subspace is then determined by means of the quasi-spherical coordinate search method [27], and the envelope surface and the stereogram of the workspace are described, defining the accessible working space for 1T2R heads as shown in Fig. 4. It can be seen from the calculation results that 1T2R head can realize the attitude space range with a maximum of $\theta \in [0°\quad 40°]$, $\psi \in [0°\quad 360°]$. As we can see from the reachable workspace, not all regions can achieve the maximum nutation angle.

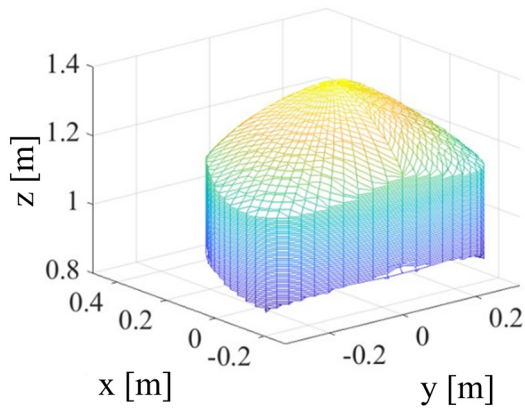

Fig. 4. *Reachable workspace of 1T2R*

3 POSE DETERMINATION AND SIMPLIFICATION ALGORITHM

By analysing and summarizing the motion rules of 1T2R head, a simplified algorithm for judging the position and pose of 1T2R parallel power head is derived. This algorithm can realize the fast response of the limit protection function under the existing hardware configuration and is used to realize the limit protection of the 1T2R head.

To facilitate calculation, the relationship between the coordinates of the tool reference point in the z and

the coordinates $z_{O'}$ of the geometric centre point of the moving platform in the direction of z is:

$$z = z_{O'} + e\cos\theta. \tag{11}$$

Thus, the input parameters of the inverse kinematics model of the 1T2R head are replaced by the coordinates of the geometric centre point O' of the moving platform in the z direction, the process angle ψ and the nutation angle θ.

Q is defined as the kinematic chain length of the branch chain movement; Q' is the difference between the kinematic chain lengths of any two branch chains.

3.1 Position Constraint Condition

As shown in Fig. 2, let the vector from the geometric centre point O of the static platform to the geometric centre point O' of the moving platform be $\mathbf{o}$. $\mathbf{r}_P$ can be expressed as

$$\mathbf{r}_P = \mathbf{o} + e\mathbf{w}. \tag{12}$$

Substituting Eq. (12) into Eq. (3), we obtain:

$$q_i\mathbf{w}_i = \mathbf{a}_i - \mathbf{b}_i + \mathbf{o} \quad i = 1,2,3\,. \tag{13}$$

By summing the above equation in order of i, and taking into account the geometric relation of the prototype $\mathbf{a}_1+\mathbf{a}_2+\mathbf{a}_3=\mathbf{b}_1+\mathbf{b}_2+\mathbf{b}_3=\mathbf{0}$, we obtain:

$$\left|q_1\mathbf{w}_1+q_2\mathbf{w}_2+q_3\mathbf{w}_3\right| = 3\left|\mathbf{o}\right|. \tag{14}$$

According to Eq. (13), the left side of the above equation is equal to $\mathbf{a}_1+\mathbf{a}_2+\mathbf{a}_3=\mathbf{b}_1+\mathbf{b}_2+\mathbf{b}_3=\mathbf{0}$; therefore:

$$\begin{aligned}&\left|q_1\mathbf{w}_1\right|+\left|q_2\mathbf{w}_2\right|+\left|q_3\mathbf{w}_3\right| \le \\ &3\left|\mathbf{o}\right|+\left|\mathbf{a}_1-\mathbf{b}_1\right|+\left|\mathbf{a}_2-\mathbf{b}_2\right|+\left|\mathbf{a}_3-\mathbf{b}_3\right|.\end{aligned} \tag{15}$$

Because $|\mathbf{a}_1-\mathbf{b}_1|+|\mathbf{a}_2-\mathbf{b}_2|+|\mathbf{a}_3-\mathbf{b}_3|$ has a maximum value of $6a\sin(\theta_{\max}/2)$ at the maximum nutation angle, the following can be obtained by sorting:

$$\left(\left|\mathbf{a}_1-\mathbf{b}_1\right|+\left|\mathbf{a}_2-\mathbf{b}_2\right|+\left|\mathbf{a}_3-\mathbf{b}_3\right|\right)_{\max} = 6a\sin\left(\theta_{\max}/2\right). \tag{16}$$

By combining Eq. (15) and Eq. (15), and substituting $|q_1\mathbf{w}_1|+|q_2\mathbf{w}_2|+|q_3\mathbf{w}_3|=Q$, the following is obtained:

$$3\left|\mathbf{o}\right| \le Q \le 3\left|\mathbf{o}\right| + 6a\sin\left(\theta_{\max}/2\right). \tag{17}$$

It can be seen from Eq. (17) that, theoretically, the sum of kinematic chains of the 1T2R power head branch prismatic pair is always approximately three times the distance from the geometric centre point of the static platform to the geometric centre point of the moving platform.

3.2 Pose Constraint Condition

A similar calculation is used for the difference of length between any two branch chains. The length difference between branched chains 1 and 2 is used as an example, which can be determined from Eq. (13):

$$q_1\mathbf{w}_1 - q_2\mathbf{w}_2 = \mathbf{a}_1 - \mathbf{a}_2 - \mathbf{b}_1 + \mathbf{b}_2. \tag{18}$$

The difference between the two sides of a triangle is less than the third:

$$\left\|q_1\mathbf{w}_1\right| - \left|q_2\mathbf{w}_2\right\| \le \left|q_1\mathbf{w}_1 - q_2\mathbf{w}_2\right|. \tag{19}$$

Substitute Eq. (23) into, and we obtain:

$$\left\|q_1\mathbf{w}_1\right| - \left|q_2\mathbf{w}_2\right\| \le \left|\mathbf{a}_1 - \mathbf{a}_2 - \mathbf{b}_1 + \mathbf{b}_2\right|, \tag{20}$$

because $\mathbf{a}_1=a\mathbf{R}\mathbf{V}_1$, $\mathbf{a}_2=a\mathbf{R}\mathbf{V}_2$, $\mathbf{b}_1=b\mathbf{V}_1$, $\mathbf{b}_2=b\mathbf{V}_2$, $\mathbf{V}_i = [\cos\varphi_i \quad \sin\varphi_i \quad 0]^{\mathrm{T}}$, $i=1,2$.

According to the actual parameters of the mechanism, $a=b$ is substituted, and then:

$$\begin{aligned}&\left|\mathbf{a}_1 - \mathbf{a}_2 - \mathbf{b}_1 + \mathbf{b}_2\right| = \\ &= a\left|(\mathbf{R}-\mathbf{E})\mathbf{T}\right| \le 2a\left(1-\cos\left(\varphi_1-\varphi_2\right)\right)\left|\mathbf{R}-\mathbf{E}\right|,\end{aligned} \tag{21}$$

where, $\mathbf{E}$ is identity matrix,
$\mathrm{T}=[\cos\varphi_1-\cos\varphi_2 \quad \sin\varphi_1-\sin\varphi_2 \quad 0]^{\mathrm{T}}$.

According to Eq. (1), the matrix $\mathbf{R}$ is related to the precession angle ψ, nutation angle θ and spin angle ϕ, and further:

$$\left|\mathbf{a}_1 - \mathbf{a}_2 - \mathbf{b}_1 + \mathbf{b}_2\right| = 2a\left(1-\cos\left(2\pi/3\right)\right) f\left(\psi,\theta\right). \tag{22}$$

Substituting Eq. (22) into Eq. (21), we obtain:

$$\left\|q_1\mathbf{w}_1\right| - \left|q_2\mathbf{w}_2\right\| \le 2a\left(1-\cos\left(2\pi/3\right)\right) f\left(\psi,\theta\right). \tag{23}$$

According to Eq. (26), we then obtain:

$$\left|Q'\right| \le 2a\left(1-\cos\left(2\pi/3\right)\right) f\left(\psi,\theta\right). \tag{24}$$

It can be seen from Eq. (24) that, theoretically, the upper bound of the length difference between any two branching chains of the 1T2R head is a function of ψ and θ.

3.3 Simulation

The form of motion in which the tool makes an arc trajectory parallel to the plane of the static platform is relatively simple and easy to describe. Therefore, under this motion, the above conclusions are verified by combining the existing 1T2R parallel mechanism data. When the values of $z_{O'}$ and θ remain unchanged at $\psi \in [0°\ \ 360°]$, the length of 1T2R head branch chain prismatic pair is calculated as shown in Fig. 5.

Since the leg length data q_1, q_2 and q_3 satisfy the symmetric three-phase sine quantity. The values of $z_{O'}$ and θ can be changed and the leg length data summed to obtain Table 2. The difference of the leg length data is taken to obtain Table 3.

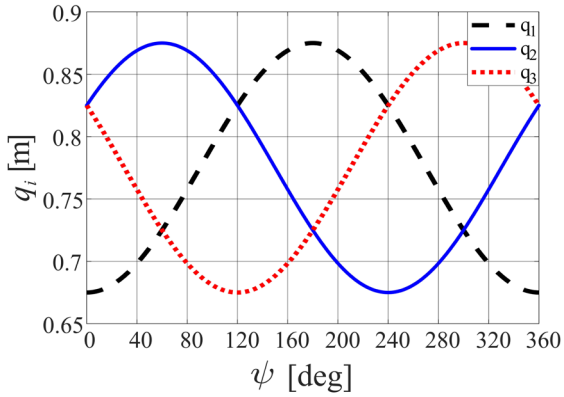

Fig. 5. *Data distribution type of 1T2R branches' length*

Table 2. *Summation of 1T2R head branches' length*

		$\theta=39$	$\theta=29°$	$\theta=19°$	$\theta=9°$	$\theta=0°$	max/min
1.8720	$Q_{\max}$	1.879424	1.874194	1.872384	1.872018	1.872000	1.879424
	$Q_{\min}$	1.876457	1.873482	1.872296	1.872016	1.872000	1.872000
1.9695	$Q_{\max}$	1.976447	1.971561	1.969863	1.969517	1.969500	1.976447
	$Q_{\min}$	1.973780	1.970920	1.969783	1.969515	1.969500	1.969500
2.0670	$Q_{\max}$	2.073528	2.068943	2.067343	2.067016	2.067000	2.073528
	$Q_{\min}$	2.071116	2.068363	2.067271	2.067015	2.067000	2.067000
2.1645	$Q_{\max}$	2.170656	2.166338	2.164826	2.164516	2.164500	2.170656
	$Q_{\min}$	2.168465	2.165811	2.164760	2.164514	2.164500	2.164500
2.2620	$Q_{\max}$	2.267824	2.263744	2.262310	2.262015	2.262000	2.267824
	$Q_{\min}$	2.265824	2.263262	2.262250	2.262013	2.262000	2.262000

Table 3. *Subtraction of any two 1T2R head branches' length*

$z_{O'}$		$\theta=39$	$\theta=29°$	$\theta=19°$	$\theta=9°$	$\theta=0°$
0.6240	$Q'_{\max}$	0.271960	0.209725	0.140941	0.067737	0
	$Q'_{\min}$	-0.271960	-0.209725	-0.140941	-0.067737	0
0.6565	$Q'_{\max}$	0.272005	0.209745	0.140944	0.067737	0
	$Q'_{\min}$	-0.272005	-0.209745	-0.140944	-0.067737	0
0.6890	$Q'_{\max}$	0.272056	0.209763	0.140947	0.067737	0
	$Q'_{\min}$	-0.272056	-0.209763	-0.140947	-0.067737	0
0.7215	$Q'_{\max}$	0.272098	0.209779	0.140950	0.067737	0
	$Q'_{\min}$	-0.272098	-0.209779	-0.140950	-0.067737	0
0.7540	$Q'_{\max}$	0.272134	0.209793	0.140952	0.067737	0
	$Q'_{\min}$	-0.272134	-0.209793	-0.140952	-0.067737	0
Average value	$Q'_{\max}$	0.272051	0.209761	0.140947	0.067737	0
	$Q'_{\min}$	-0.272051	-0.209761	-0.140947	-0.067737	0

According to the data of Fig. 5 and Table 2, the following relationship can be fit:

$$\underline{Q} \le Q \le \overline{Q}, \tag{25}$$

where, $\underline{Q}$ represents the lower bound of the length sum of the branch chain movement, $\underline{Q} = 3z_{O'}$, $\overline{Q}$ represents the upper bound of the length sum of the branch chain movement

$$\overline{Q} = 3z_{O'} - 0.012251z_{O'} + 0.015190\,.$$

From the data in Table 2 and the Eq. (25), it can be seen that the length of the 1T2R head branch chain prismatic pair is always approximately equal to three times of $z_{O'}$, which satisfies the Eq. (21). Therefore, the motion characteristic law of this form of motion can be extended.

By the same token, through Fig. 5 and Table 3, Q' and θ can be fitted as follows:

$$|Q'| \le \overline{Q'}, \tag{26}$$

where, $\overline{Q'}$ represents the upper bound of the length difference $|Q'|$ of the auxiliary leg of the branch chain movement, $\overline{Q'} \le 0.006997\theta + 0.003748$.

It can be seen from Eq. (26) that in the case of the same nutation angle, the upper bound of the difference between the length of any two kinematic chains is almost the same, with only an error of orders of magnitude. This satisfies Eq. (24). Therefore, the motion characteristic law of this form of motion can be extended.

The above is the analysis of the motion characteristics of a 1T2R head and the simplified algorithm of pose judgment. The aim of the algorithm is to further divide the working space of the mechanism through the information of the three branch chains, so that the judgment of the attitude of the mechanism can be obtained without establishing a complex mapping model of the servo motor action. Within its workspace, the sum length of the 1T2R head branch chain prismatic pair is always approximately equal to three times the coordinate value of the geometric centre of the moving platform. The absolute value of the difference between the lengths of any two branch chains is always less than a specific value related to the nutation angle. Thus, the limit protection of 1T2R head can be realized simply, reliably, and efficiently.

4 LIMIT PROTECTION IMPLEMENTATION PROCESS

Based on the above analysis results of the movement characteristics of a 1T2R power head, the simplified algorithm of position and pose judgment, the limit protection method is designed in combination with the actual mechanical structure of the 1T2R power head servo feed system and its control system. This method will adopt two methods: proactive limit and preventive limit.

The active limits are all areas of the 1T2R power head dexterous workspace except the boundary. The preventive limits are to prevent the mechanism from exceeding the workspace boundary, i.e., the boundary area of the 1T2R power head dexterous workspace. Real-time data of the prismatic pair length of the branch chain can be obtained through the feedback signal of the encoder of the servo motor. The PLC program in the motion controller PMAC is used to sum the leg lengths of the three branches and calculate the difference between the lengths of any two branches. The results of the operation are fed into the motion controller register. Then, according to the above pose judgment algorithm, whether the limit area is exceeded can be determined. The specific realization method of the 1T2R power head limit is shown in Fig. 6.

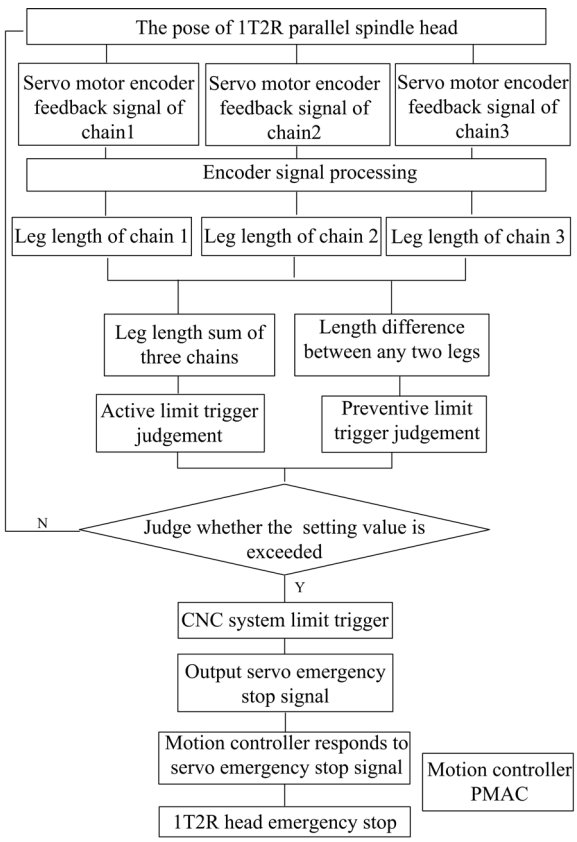

Fig. 6. *Schematic diagram of limit protection process*

For the active limit, according to Table 2, $Q_{\min} = 1.872000$ is determined to be the lower trigger condition value of the active limit, and $Q_{\max} = 2.267824$ is determined to be the upper trigger condition value of the active limit. For the preventive limit position, according to the data shown in Table 3, it is determined that $Q'_{\max} = 1.272134$ is the upper limit trigger condition value of the preventive limit position, and $Q'_{\min} = -0.272134$ is the lower limit trigger condition value of the preventive limit position.

5 EXPERIMENTAL ANALYSIS

The experimental platform is shown in Fig. 7, and the 1T2R parallel power head is driven by three chains. Fig. 8 shows the servo feed control system. The real-time length of three branches can be obtained through the code disk of the branch servo motor. The trajectory is an approximately circular trajectory parallel to the plane of the static platform, as shown in Fig. 9. According to the scale parameters (a, b, l, e) mentioned above, after consulting the machine tool operation manual, it is found that collision interference occurs easily when the nutation angle is 40°, so the nutation angle θ is selected as 30°. The motion position of the tool reference point P at the end of the mechanism in the z direction is 1.1687 m, the nutation angle θ is 30°, and the precession angle ψ is varied from 0° to 360°. The length data of each chain obtained during the experiment are shown in Table 4. Fig. 10 shows the variation rule of the length of the branch chain corresponding to the trajectory.

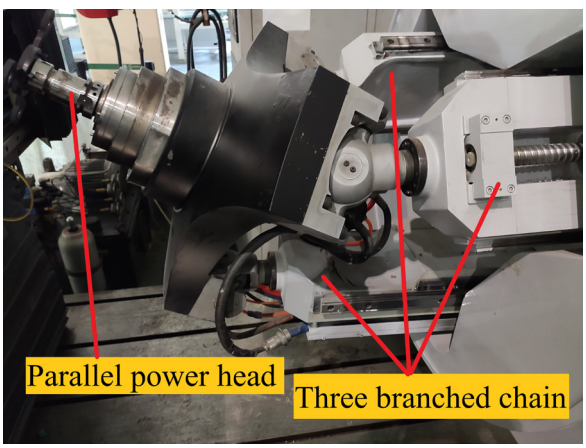

Fig. 7. *1T2R parallel power head*

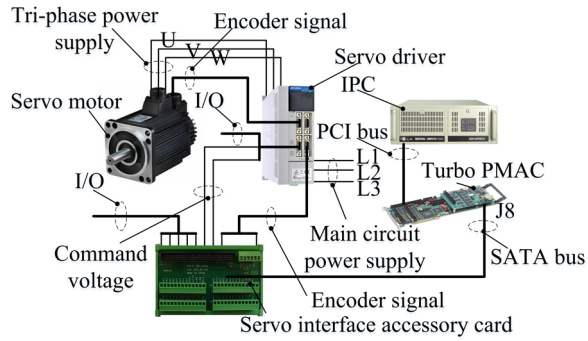

Fig. 8. *Servo feed control system*

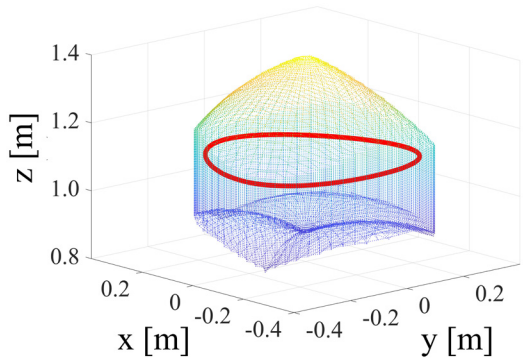

Fig. 9. *Schematic diagram of trajectory reachable workspace*

Fig. 11a shows the numerical distribution law after the summation of the length data of the motion track. It can be seen from the distribution of the summation result that the sum of the length is distributed within the interval range of 2.2514 m to 2.2521 m and has periodic data fluctuation with a small amplitude. As shown in Fig. 11b, in comparing the length of the data points and the result data with the threshold value of the over-limit setting, it is found that none of the data points in the trajectory exceed the limit.

Table 4. *Experimental kinematic chain length data*

t [s]	0.0000	0.0221	0.0443	0.0664	0.0885	0.1107	0.1328	0.1549
q_1 [m]	0.6269	0.627	0.627	0.627	0.627	0.627	0.627	0.6271
q_2 [m]	0.8121	0.8121	0.8118	0.8114	0.811	0.8106	0.8101	0.8097
q_3 [m]	0.8123	0.8128	0.8132	0.8136	0.814	0.8144	0.8149	0.8153
t [s]	0.1771	0.1992	0.2214	0.2435	0.2656	0.2878	0.3099	…
q_1 [m]	0.6271	0.6271	0.6271	0.6271	0.6271	0.6272	0.6272	…
q_2 [m]	0.8093	0.8089	0.8084	0.8080	0.8076	0.8071	0.8067	…
q_3 [m]	0.8157	0.8161	0.8165	0.8169	0.8173	0.8177	0.8181	…
t [s]	35.9922	36.0143	36.0365	36.0586	36.0807	36.1029	36.1250	36.1471
q_1 [m]	0.627	0.627	0.627	0.627	0.627	0.627	0.627	0.627
q_2 [m]	0.8129	0.8126	0.8125	0.8125	0.8125	0.8125	0.8125	0.8125
q_3 [m]	0.8121	0.8124	0.8125	0.8125	0.8125	0.8125	0.8125	0.8125

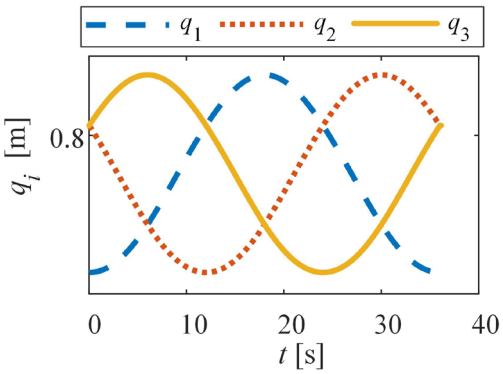

Fig. 10. *Branches' length variation law*

Fig. 12a shows the numerical distribution of the leg length difference of any two branch chains. It can be seen from the distribution of the difference results that the leg length has a periodic fluctuation with a fluctuation range of 0 m to 0.2164 m, and the distribution form of the difference results of different branch leg lengths is the same except for the phase differences. As shown in Fig. 12b, by comparing the result data of the leg length difference of data points with the threshold value of the over-limit setting, it can be seen that none of the data points in the trajectory exceed the limit.

Through the above simulation verification of the simplification algorithm of pose judgment, it is proved that the simplification algorithm of pose judgment can realize real-time judgment of the terminal pose state of the mechanism during the action process of a 1T2R power head. The result of pose judgment of this algorithm is found to be accurate. The active limit and preventive limit set according to the simplified algorithm of position and pose judgment can realize the limit protection function of 1T2R mechanism accurately and reliably and ensure the safe and reliable operation of the mechanism.

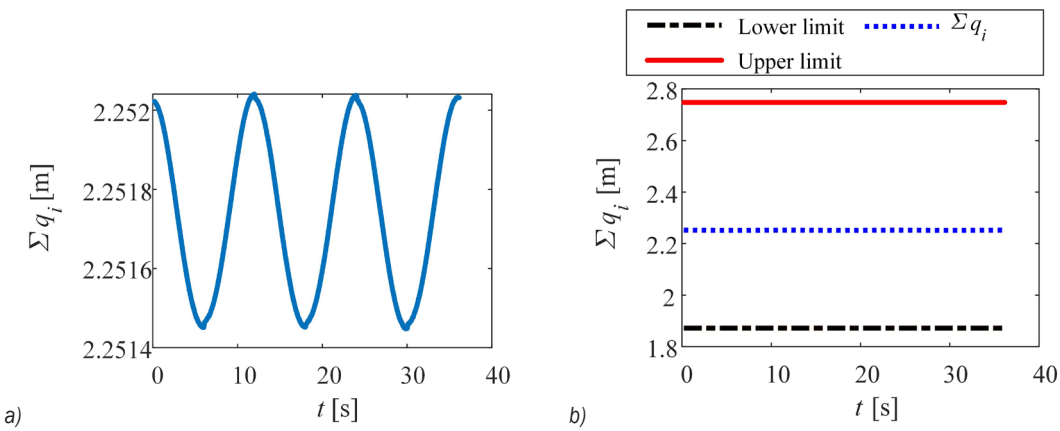

Fig. 11. *Branches' length summation distribution of data points; a) numerical distribution of the summation, and b) extra-limit judgment of summation*

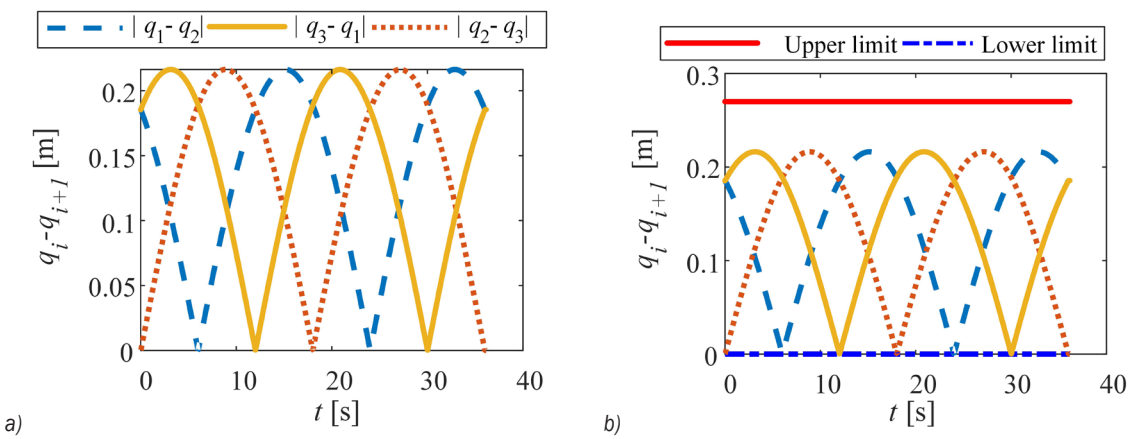

Fig. 12. *Distribution of branches' length difference; a) numerical distribution of the leg length difference, and b) extra-limit judgment of difference of leg length*

6 CONCLUSION

(1) This paper presents a simplified algorithm for the determination of the position and pose of 1T2R power head. Compared with the pose judgment method using the inverse solution model, it is estimated to be 99.42 % faster with no need to upgrade the original system. The simplified algorithm is easy to implement, efficient and reliable.

(2) The real-time limit protection of a 1T2R power head can be realized simply and reliably with the help of the simplification algorithm of position and pose judgment. Based on the software and hardware conditions of the existing numerical control system, this method can effectively solve the real-time limit protection problem of parallel machine tools by combining software and hardware and improve the operation safety of such topological machine tools.

7 ACKNOWLEDGEMENTS

The authors would like to acknowledge the financial supported from the National Natural Science Foundation of China (Grant No.51575385) and National Key Research and Development Program of China (Grant No.2019YFA0709004). The authors also acknowledge Key Laboratory of Mechanism Theory and Equipment Design of Ministry of Education and School of Mechanical Engineering the in Tianjin University for providing the experimental environment.

8 REFERENCES

[1] Guo, J.Z., Wang, D., Fan, R., Chen, W.Y. (2017). Design and workspace analysis of a 3-degree-of-freedom parallel swivel head with large tilting capacity. *Proceedings of the Institution of Mechanical Engineers, Part B: Journal of Engineering Manufacture*, vol. 231, no. 10, p. 1838-1849, **DOI:10.1177/0954405415607782**.

[2] Ni, Y., Zhou, H., Shao, C., Li, J. (2019). Research on the error averaging effect in a rolling guide pair. *Chinese Journal of Mechanical Engineering*, vol. 32, art. ID. 72, **DOI:10.1186/s10033-019-0386-y**.

[3] Cheng, G., Gu, W., Yu, J.-l., Tang, P. (2011). Overall structure calibration of 3-ucr parallel manipulator based on quaternion method. *Strojniški vestnik - Journal of Mechanical Engineering*, vol. 57, no. 10, p. 719-729, **DOI:10.5545/sv-jme.2010.167**.

[4] Ni, Y., Zhang, Y., Sun, K., Wang, H., Sun, Y. (2016). Interpolation control algorithm for a three-RPS parallel spindle head. *Proceedings of the Institution of Mechanical Engineers, Part I: Journal of Systems & Control Engineering*, vol. 230, no. 7, p. 661-671, **DOI:10.1177/0959651816645687**.

[5] Baizid, K., Ćukovic, S., Iqbal, J., Yousnadj, A., Chellali, R., Meddahi, A., Devedžić, G., Ghionea, I. (2016). IRoSim: Industrial robotics simulation design planning and optimization platform based on CAD and knowledgeware technologies. *Robotics and Computer-Integrated Manufacturing*, vol. 42, p. 121-134, **DOI:10.1016/j.rcim.2016.06.003**.

[6] Kumar, V. (1992). Characterization of workspaces of parallel manipulators. *Journal of Mechanical Design*, vol. 114, no. 3, p. 368-375, **DOI:10.1115/1.2926562**.

[7] Xu, P., Cheung, C.-F., Li, B., Ho, L.-T., Zhang, J.-F. (2017). Kinematics analysis of a hybrid manipulator for computer controlled ultra-precision freeform polishing. *Robotics and Computer-Integrated Manufacturing*, vol. 44, p. 44-56, **DOI:10.1016/j.rcim.2016.08.003**.

[8] Macho, E., Altuzarra, O., Amezua, E., Hernandez, A. (2009). Obtaining configuration space and singularity maps for parallel manipulators. *Mechanism & Machine Theory*, vol. 44, no. 11, p. 2110-2125, **DOI:10.1016/j.mechmachtheory.2009.06.003**.

[9] Huang, C.K., Tsai, K.Y. (2015). A general method to determine compatible orientation workspaces for different types of 6-DOF parallel manipulators. *Mechanism & Machine Theory*, vol. 85, no. p. 129-146, **DOI:10.1016/j.mechmachtheory.2014.11.011.**

[10] Zhang, D., Gao, Z. (2012). Optimal kinematic calibration of parallel manipulators with pseudoerror theory and cooperative coevolutionary network. *IEEE Transactions on Industrial Electronics*, vol. 59, no. 8, p. 3221-3231, **DOI:10.1109/TIE.2011.2166229**.

[11] Cui, G., Zhang, H., Zhang, D., Xu, F. (2015). Analysis of the kinematic accuracy reliability of a 3-DOF parallel robot manipulator. *International Journal of Advanced Robotic Systems*, vol. 12, no. 2, p. 15-26, **DOI:10.5772/60056**.

[12] Shao, J., Chen, W., Fu, X. (2015). Position, singularity and workspace analysis of 3-PSR-0 spatial parallel manipulator. *Chinese Journal of Mechanical Engineering*, vol. 28, p. 437-450, **DOI:10.3901/CJME.2015.0122.018**.

[13] Kaloorazi, M.H.F., Masouleh, M.T., Caro, S. (2015). Determination of the maximal singularity-free workspace of 3-DOF parallel mechanisms with a constructive geometric approach. *Mechanism & Machine Theory*, vol. 84, p. 25-36, **DOI:10.1016/j.mechmachtheory.2014.10.003**.

[14] Zhang, D., Wei, B. (2017). Interactions and optimizations analysis between stiffness and workspace of 3-UPU robotic mechanism. *Measurement Science Review*, vol. 17, no. 2, p. 83-92, **DOI:10.1515/msr-2017-0011**.

[15] Gao, Z., Zhang, D. (2011). Workspace representation and optimization of a novel parallel mechanism with three-degrees-of-freedom. *Sustainability*, vol. 3, no. 11, p. 2217-2228, **DOI:10.3390/su3112217**.

[16] Zhu, C., Guan, L., Han, J., Wang, L. (2009). A new resolution of workspace problem of parallel machine tool. *IEEE International Conference on Automation and Logistics*, p. 1002-1007, **DOI:10.1109/ICAL.2009.5262566**.

[17] FarzanehKaloorazi, M.H., Masouleh, M.T., Caro, S. (2017). Collision-free workspace of parallel mechanisms based on an interval analysis approach. *Robotica*, vol. 35, no. 8, p. 1747-1760, **DOI:10.1017/S0263574716000497**.

[18] Majid, M.Z.A., Huang, Z., Yao, Y.L. (2000). Workspace analysis of a six-degrees of freedom, three-prismatic-prismatic-

spheric-revolute parallel manipulator. *International Journal of Advanced Manufacturing Technology*, vol. 16, p. 441-449, **DOI:10.1007/s001700050176**.

[19] Rouhani, E., Nategh, M.J. (2015). Workspace, dexterity and dimensional optimization of microhexapod. *Assembly Automation*, vol. 35, no. 4, p. 341-347, **DOI:10.1108/AA-03-2015-020**.

[20] Wan, J., Yao, J., Zhang, L., Wu, H. (2018). A weighted gradient projection method for inverse kinematics of redundant manipulators considering multiple performance criteria. *Strojniški vestnik - Journal of Mechanical Engineering*, vol. 64, no. 7-8, p. 475-487, **DOI:10.5545/sv-jme.2017.5182**.

[21] Khoukhi, A., Baron, L., Balazinski, M. (2009). Constrained multi-objective trajectory planning of parallel kinematic machines. *Robotics and Computer-Integrated Manufacturing*, vol. 25, no. 4-5, p. 756-769, **DOI:10.1016/j.rcim.2008.09.002**.

[22] Reveles, R.D., Pamanes, G.J.A., Wenger, P. (2016). Trajectory planning of kinematically redundant parallel manipulators by using multiple working modes. *Mechanism and Machine Theory*, vol. 98, p. 216-230, **DOI:10.1016/j.mechmachtheory.2015.09.011**.

[23] Dash, A.K., Chen, I.-M., Yeo, S.H., Yang, G. (2005). Workspace generation and planning singularity-free path for parallel manipulators. *Mechanism and Machine Theory*, vol. 40, no. 7, p. 776-805, **DOI:10.1016/j.mechmachtheory.2005.01.001**.

[24] Iqbal, J., Ullah, M.I., Khan, A.A., Irfan, M. (2015). Towards sophisticated control of robotic manipulators: An experimental study on a pseudo-industrial arm. *Strojniški vestnik - Journal of Mechanical Engineering*, vol. 61, no. 7, p. 465-470, **DOI:10.5545/sv-jme.2015.2511**.

[25] Manzoor, S., Islam, R.U., Khalid, A., Samad, A., Iqbal, J. (2014). An open-source multi-DOF articulated robotic educational platform for autonomous object manipulation. *Robotics and Computer-Integrated Manufacturing*, vol. 30, no. 3, p. 351-362, **DOI:10.1016/j.rcim.2013.11.003**.

[26] Alam, W., Mehmood, A., Ali, K., Javaid, U., Alharbi, S., Iqbal, J. (2018). Nonlinear control of a flexible joint robotic manipulator with experimental validation. *Strojniški vestnik - Journal of Mechanical Engineering*, vol. 64, no. 1, p. 47-55, **DOI:10.5545/sv-jme.2017.4786**.

[27] Mahmoodi, A., Sayadi, A.. (2015). Six-Dimensional space expression of workspace of six-DoF parallel manipulators using hyper spherical coordinates (HSC). *Advanced Robotics,* vol. 29, no. 23, p. 1527-1537, **DOI:10.1080/01691864.2015.1076345**.